Pair dynamics in a glass-forming binary mixture: Simulations and theory

Rajesh K. Murarka and Biman Bagchi*
Solid State and Structural Chemistry Unit, Indian Institute of Science, Bangalore, India 560 012

We have carried out molecular dynamics simulations to understand the dynamics of a *tagged pair of atoms* in a strongly nonideal glass-forming binary Lennard-Jones mixture. Here atom B is smaller than atom A ($\sigma_{BB}=0.88\sigma_{AA}$, where σ_{AA} is the molecular diameter of the A particles) and the AB interaction is stronger than that given by Lorentz-Berthelot mixing rule ($\epsilon_{AB}=1.5\epsilon_{AA}$, where ϵ_{AA} is the interaction energy strength between the A particles). The generalized time-dependent pair distribution function is calculated separately for the three pairs (AA, BB, and AB). The three pairs are found to behave differently. The relative diffusion constants are found to vary in the order $D_R^{BB}>D_R^{AB}>D_R^{AA}$, with $D_R^{BB}\simeq 2D_R^{AA}$, showing the importance of the hopping process (B hops much more than A). We introduce a *non-Gaussian parameter* $[\alpha_2^P(t)]$ to monitor the relative motion of a pair of atoms and evaluate it for all the three pairs with initial separations chosen to be at the first peak of the corresponding partial radial distribution functions. At intermediate times, significant deviation from the Gaussian behavior of the pair distribution functions is observed with different degrees for the three pairs. A simple mean-field (MF) model, proposed originally by Haan [Phys. Rev. A **20**, 2516 (1979)] for one-component liquid, is applied to the case of a binary mixture and compared with the simulation results. While the MF model successfully describes the dynamics of the AA and AB pairs, *the agreement for the BB pair is less satisfactory*. This is attributed to the large scale anharmonic motions of the B particles in a weak effective potential. Dynamics of the next nearest neighbor pairs is also investigated.

I. INTRODUCTION

In dense fluids, there are many interaction-induced phenomena that can be interpreted in terms of the dynamics of the pairs of atoms [1–3]. For example, nuclear overheusser effect studies the relative motion of the atoms. In addition, an understanding of pair dynamics can be of great importance in the studies of rate of various diffusion controlled chemical reactions in dense fluids [4,5]. Both the theoretical analysis [1,6–11] and computer simulation studies [6,8–10,12] have been carried out extensively to study the dynamics of a pair of atoms in a one-component liquid. Surprisingly, however, we are not aware of any explicit study on the dynamics of atomic pairs in binary mixtures, whose dynamics generally shows strong nonmonotonic composition dependence [13,14].

The study of the electronic spectroscopy of dilute chromophores (solutes) in fluids (solvents) is a useful tool for obtaining the information about the structure and dynamics of the solvents in the vicinity of the solute. In an attempt to provide a microscopic foundation of the Kubo's stochastic theory of the line shape, Skinner and co-workers [15] have recently developed a molecular theory for the absorption and emission line shapes and ultrafast solvation dynamics of a dilute nonpolar solute in nonpolar fluids. Due to the motion of the solvent molecules relative to the chromophore, the chromophore's transition frequency generally fluctuates in time. Thus, the nature of the spectral line shape provides a useful information about the details of the dynamics of the solvent relative to the solute. An approximate treatment of the solvent dynamics allowed the theory to express the transition frequency fluctuation time correlation functions (related to the expressions for the absorption and emission line shapes) solely in terms of the two-body solute-solvent time-dependent conditional pair distribution function. Many other applications of pair dynamics have been discussed by a number of authors [6,8,10,11,16].

The dynamics of a liquid below its freezing temperature, i.e., in a supercooled state, is far more complex than what one would expect from an extrapolation of their high-temperature behavior. One of the most challenging problems in the dynamics of a supercooled liquid is to understand quantitatively the origin of the nonexponential relaxation exhibited by various dynamical response functions and the extraordinary viscous slow down within a narrow temperature range as one approaches the glass transition temperature from above [17,18]. Many experimental studies [19,20] as well as computer simulations [21–24] have been performed to shed light on the underlying microscopic mechanism involved in supercooled liquids. These studies have revealed evidence of the presence of distinct relaxing domains (spatial heterogeneity), which is thought to be responsible for the nonexponential relaxations in deeply supercooled liquids. Molecular motions in strongly supercooled liquid involve highly collective movement of several molecules [22,25–28]. Furthermore, the correlated jump motions become the dominant diffusive mode [28,29]. The observed heterogeneity of the relaxations in a deeply supercooled liquid is found to be connected to the collective hopping of groups of particles [30].

The occurrence of increasingly heterogeneous dynamics in supercooled liquids, however, has been investigated solely in terms of single-particle dynamics. The study of the dynamics of pair of atoms that involve higher-order (two-body) correlations thus can provide much broader insight into the

*Email address: bbagchi@sscu.iisc.ernet.in

anomalous dynamics of supercooled liquids. In this work, we have carried out molecular dynamics simulations in a strongly nonideal glass-forming binary mixture (commonly known as Kob-Andersen model [21]) to study the relaxation mechanism in terms of pair dynamics. The main purpose of the present study is to explore the dynamics in a more collective sense by following the relative motion of three different types (AA, BB, and AB) of nearest neighbor and next nearest neighbor pair of atoms. These three pairs are found to behave differently. The simulation results show a clear signature of hopping motion in all the three pairs. We have also performed simple mean-field (MF) model (as introduced by Haan [6] for one component liquid) calculations to obtain the time-dependent conditional pair distribution functions.

The organization of the rest of the paper is as follows. In Sec. II, we describe the details of the simulation and the model system used in this study. The simulation results are presented and discussed in Sec. III. In Sec. IV, we have presented a mean-field model calculations for pair dynamics in a binary mixture and the comparison is made with the simulation results. Finally, a few concluding remarks are presented in Sec. V.

II. SYSTEM AND SIMULATION DETAILS

We have performed equilibrium isothermal-isobaric ensemble (N-P-T) molecular dynamics (MD) simulations of a strongly nonideal well-known glass-forming binary mixture in three dimensions. The binary system studied here contains a total of $N=1000$ particles consisting of two species of particles, A and B with $N_A=800$ and $N_B=200$ number of A and B particles, respectively. Thus, the mixture consists of 80% of A particles and 20% of B particles. The interaction between any two particles is modeled by shifted force Lennard-Jones (LJ) pair potential [31], where the standard LJ is given by

$$u_{ij}^{LJ}=4\epsilon_{ij}\left[\left(\frac{\sigma_{ij}}{r_{ij}}\right)^{12}-\left(\frac{\sigma_{ij}}{r_{ij}}\right)^{6}\right], \tag{1}$$

where i and j denote two different particles (A and B). The potential parameters are as follows: $\epsilon_{AA}=1.0$, $\sigma_{AA}=1.0$, $\epsilon_{BB}=0.5$, $\sigma_{BB}=0.88$, $\epsilon_{AB}=1.5$, and $\sigma_{AB}=0.8$. The mass of the two species is same ($m_A=m_B=m$). Note that in this model system, the AB interaction (ϵ_{AB}) is much stronger than both of their respective pure counterparts and σ_{AB} is smaller than what is expected from the Lorentz-Berthelot mixing rules. In order to lower the computational burden, the potential has been truncated with a cutoff radius of $2.5\sigma_{AA}$. All the quantities in this study are given in reduced units, such as length in units of σ_{AA}, temperature T in units of ϵ_{AA}/k_B, and pressure P in units of $\epsilon_{AA}/\sigma_{AA}^3$. The corresponding microscopic time scale is $\tau=\sqrt{m\sigma_{AA}^2/\epsilon_{AA}}$.

Simulations in the N-P-T ensemble are performed using the Nose-Hoover-Andersen method [32], where the external reduced temperature is held fixed at $T^*=1.0$. The external reduced pressure has been kept fixed at $P^*=20.0$. The reduced average density $\overline{\rho}^*(=\overline{\rho}\sigma_{AA}^3)$ of the system corresponding to this thermodynamic state point is 1.32. Throughout the course of the simulations, the barostat and the system's degrees of freedom are coupled to an independent Nose-Hoover chain (NHC) [33] of thermostats, each of length five. The extended system equations of motion are integrated using the reversible integrator method [34] with a time step of 0.002. The higher-order multiple time step method has been employed in the NHC evolution operator which leads to stable energy conservation for non-Hamiltonian dynamical systems [35]. The extended system time scale parameter used in the calculations is taken to be 1.15 for both the barostat and thermostats.

The system is equilibrated for 2×10^6 time steps and the simulation is carried out for another 10^7 production steps, during which the quantities of interest are calculated.

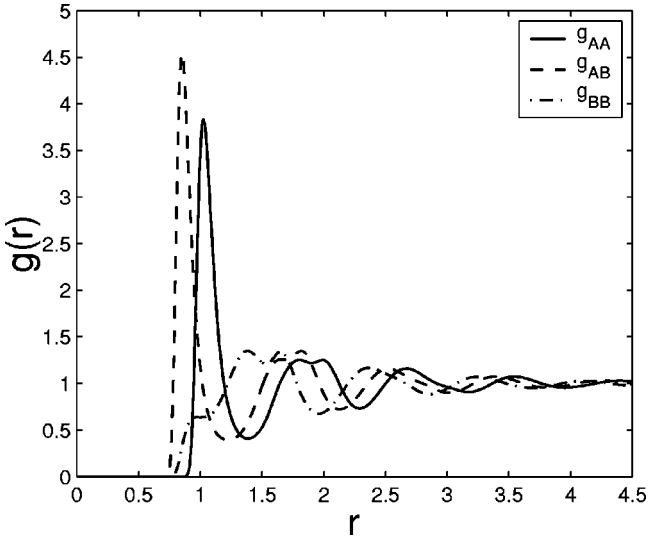

FIG. 1. The radial distribution function $g(r)$ for the AA, AB, and BB correlations is plotted against distance. The solid line is $g_{AA}(r)$, the dashed line is $g_{AB}(r)$, and the dot-dashed line is $g_{BB}(r)$. For details, see the text.

III. SIMULATION RESULTS AND DISCUSSION

The three partial radial distribution functions $g_{AA}(r)$, $g_{AB}(r)$, and $g_{BB}(r)$ obtained from simulations are plotted in Fig. 1. Due to the strong mutual interaction, the AB correlation is obviously the strongest among the three pairs. The splitting of the second peak of both $g_{AA}(r)$ and $g_{AB}(r)$ is a characteristic signature of dense random packing. The structure of $g_{BB}(r)$ is interestingly different. It has an insignificant first peak that originates from the weak interaction between the B-type particles. The second peak of $g_{BB}(r)$ is higher than that of the first peak signifying that the predominant BB correlation takes place at the second coordination shell. The occurrence of the splitted second peak is clearly observed here also.

In the present study, the central quantity of interest is the *time-dependent pair distribution function* (TDPDF) (first introduced by Oppenheim and Bloom [1] in the theory of nuclear spin relaxation in fluids), $g_2(\mathbf{r}_o,\mathbf{r};t)$ which is the conditional probability that two particles are separated by $\mathbf{r}$ at time t if that pair were separated by $\mathbf{r}_o$ at time $t=0$. Thus,

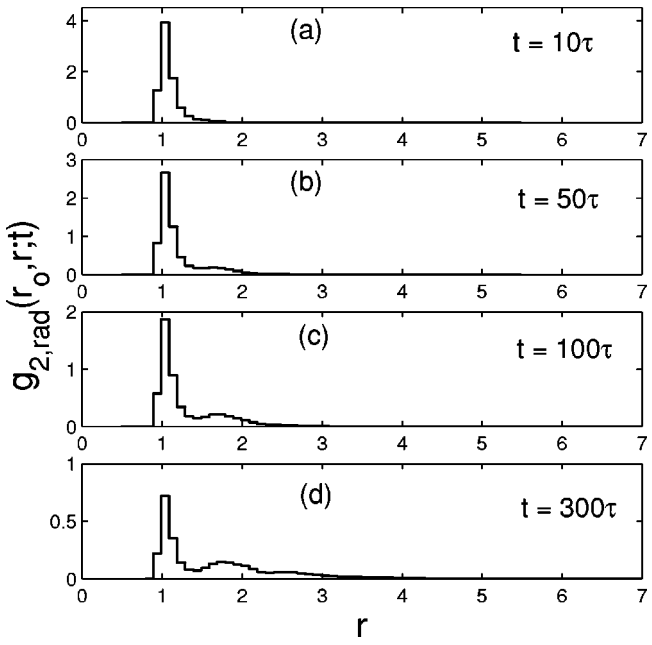

FIG. 2. The radial part of the time-dependent pair distribution function $g_{2,rad}(r_o,r;t)$ for the AA pair as a function of separation r at four different times: (a) $t=20\tau$, (b) $t=50\tau$, (c) $t=100\tau$, and (d) $t=300\tau$. The initial separation r_o corresponds to the first maximum of $g_{AA}(r)$. Note that the time unit $\tau=\sqrt{m\sigma_{AA}^2/\epsilon_{AA}}=2.2$ ps if argon units are assumed.

the TDPDF measures the relative motion of a pair of atoms. For an isotropic fluid, the TDPDF depends only on the magnitudes of $\mathbf{r}$, $\mathbf{r}_o$, and θ, where θ is the angle between $\mathbf{r}$ and $\mathbf{r}_o$. In computer simulations, one can readily evaluate separately the radial and orientational features of the relative motion. In the following two sections, we present, respectively, the results obtained for the time evolution of the radial part $g_{2,rad}(r_o,r;t)$ and the angular part $g_{2,ang}(r_o,\theta;t)$ of the TDPDF for the three different pairs (AA, BB, and AB).

A. Radial part of the TDPDF, $g_{2,rad}(r_o,r;t)$

In Fig. 2 we plot the $g_{2,rad}(r_o,r;t)$ for the AA pair with the initial separation r_o corresponding to the first maximum of the partial radial distribution function $g_{AA}(r)$ (i.e., the pair which is the nearest neighbor) at four different times. While at short time [Fig. 2(a)], the distribution function has a single-peak structure as expected, it reaches slowly to its asymptotic limit with an increase in time where additional peaks develop at larger relative separations [see Figs. 2(b)–2(d)]. The microscopic details of the underlying diffusive process (by which it approaches to the asymptotic structure) can be obtained by following the trajectory of the relative motions. Figure 3 displays the projections onto the x-y plane of the trajectory of a typical AA pair for the nearest neighbor A atoms over a time interval of $\Delta t=500\tau$. The motion of the AA pair is shown to be relatively localized for many time steps and then the pair move significant distances only during quick, rare cage rearrangements. This is a clear evidence that the jump motions are the dominant diffusive mode, by which the separation between pairs of atoms evolves in time.

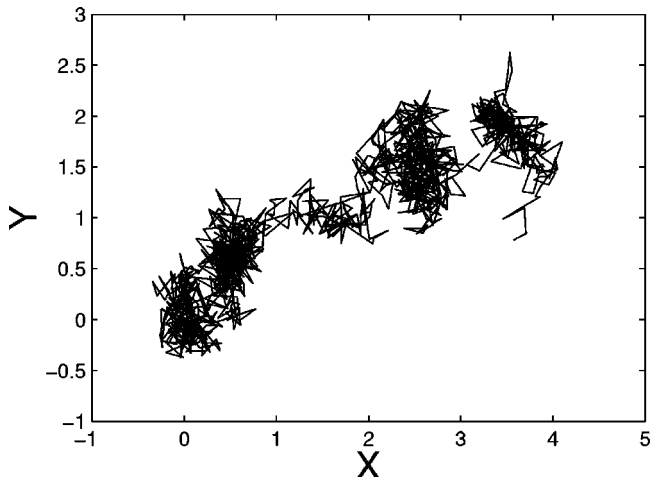

FIG. 3. Projections into x-y plane of the trajectory of a typical nearest neighbor AA pair over a time interval $t=500\tau$. Note that the time unit $\tau=2.2$ ps for argon units.

The behavior of the distribution function $g_{2,rad}(r_o,r;t)$ for the AB pair (where the interaction being the strongest) is plotted in Fig. 4 at four different times. The distribution function shows the same qualitative behavior as we observed in the case of AA correlation (Fig. 2). When compared to the AA correlation function within the same time scale, the decay of the correlation function is found to be faster despite the much strong AB interaction. This must be attributed to the difference in size of the two types of particles. As the B particles are smaller in size than the A particles, they are

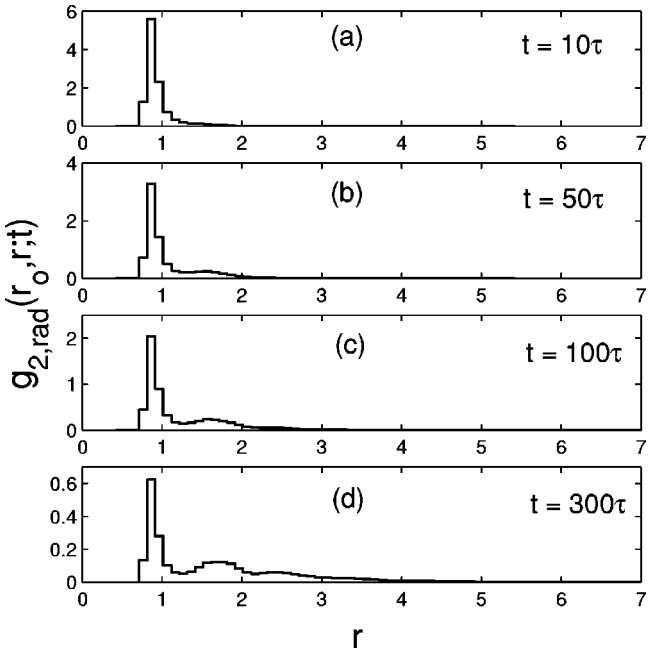

FIG. 4. The radial part of the time-dependent pair distribution function $g_{2,rad}(r_o,r;t)$ for the AB pair as a function of separation r at four different times: (a) $t=20\tau$, (b) $t=50\tau$, (c) $t=100\tau$, and (d) $t=300\tau$. The initial separation r_o corresponds to the first maximum of $g_{AB}(r)$. The time unit $\tau=2.2$ ps for the argon units. Note that $g_{2,rad}(r_o,r;t)$ is scaled by $1/\sigma_{AA}^3$. For further details, see the text.

more mobile. In addition, the AB interaction is such that AB repulsion is felt at relatively small distances ($\sigma_{AB}=0.8$ instead of 0.94 according to the Lorentz-Berthelot rules). Consequently, the B particles are more prone to make jumps than the A particles (as observed earlier by Kob and Andersen [21]).

The nature of the relative motion of a typical AB pair is illustrated in Fig. 5(a), which displays the trajectory of a typical AB pair (in the x-y plane) that was initially at the nearest neighbor [first peak of $g_{AB}(r)$]. The elapsed time is $\Delta t=500\tau$. The dynamics of the relative motion is again dominated by hopping, the AB pair remains trapped at their initial separation over hundred time steps, before jumping to neighboring sites where they again become localized. Further, the jump motion is more frequent for the AB pair than that for the AA pair. The individual trajectory of the A and B particles of the same AB pair within the same time window is shown in Figs. 5(b) and 5(c), respectively. While both A and B particles hop, B particles move faster and the effect of caging is weaker (than the A particles) due to its smaller size. In this time window, the net displacement of the AB pair in the x-y plane is found to be quite large and mainly determined by the displacement of the B particle as shown in Fig. 6.

In Fig. 7 we show $g_{2,rad}(r_o,r;t)$ for the BB pair [initially separated at the first peak of $g_{BB}(r)$] at four different times. Due to a weak interaction among B particles, one expects that the B atoms in the BB pair will fast lose the memory of their initial separation. This is indeed the case for the BB pair shown in Fig. 7. Once again the jump dynamics is clearly seen in the trajectory of a typical BB pair projected in the x-y plane (Fig. 8).

We now consider the case where the initial separation of the pairs corresponds to the second peak of their respective partial radial distribution functions in Fig. 1 (i.e., pairs which are next nearest neighbors). The distribution function for the AA pair is plotted in Fig. 9. It shows a qualitatively different behavior because the peak at the nearest neighbor separation develops in a relatively short time. Here also the motions of the pairs are found to be mostly discontinuous in nature. Thus, the motion from second to first nearest neighbor occurs mostly by hopping. In Fig. 10 we plot the similar distribution function for the AB pair. Since the AB interaction is the strongest, the height of the first peak grows faster than that for the AA pair [compare Figs. 9(b) and 10(b)]. Next, in Fig. 11 we plot the distribution function for the BB pair. Contrary to the AA and AB pairs, the BB pair tends to retain its initial separation for a relatively long time compared to the nearest neighbor pair. This can be understood from the predominant BB correlations at the second coordination shell.

B. Angular part of the TDPDF, $g_{2,ang}(r_o,\theta;t)$

In this section, we present the *angular distribution function* $g_{2,ang}(r_o,\theta;t)$ for the three different pairs (AA, BB, and AB). The initial separation r_o for the three pairs corresponds to the first peak of the respective partial radial distribution functions (Fig. 1).

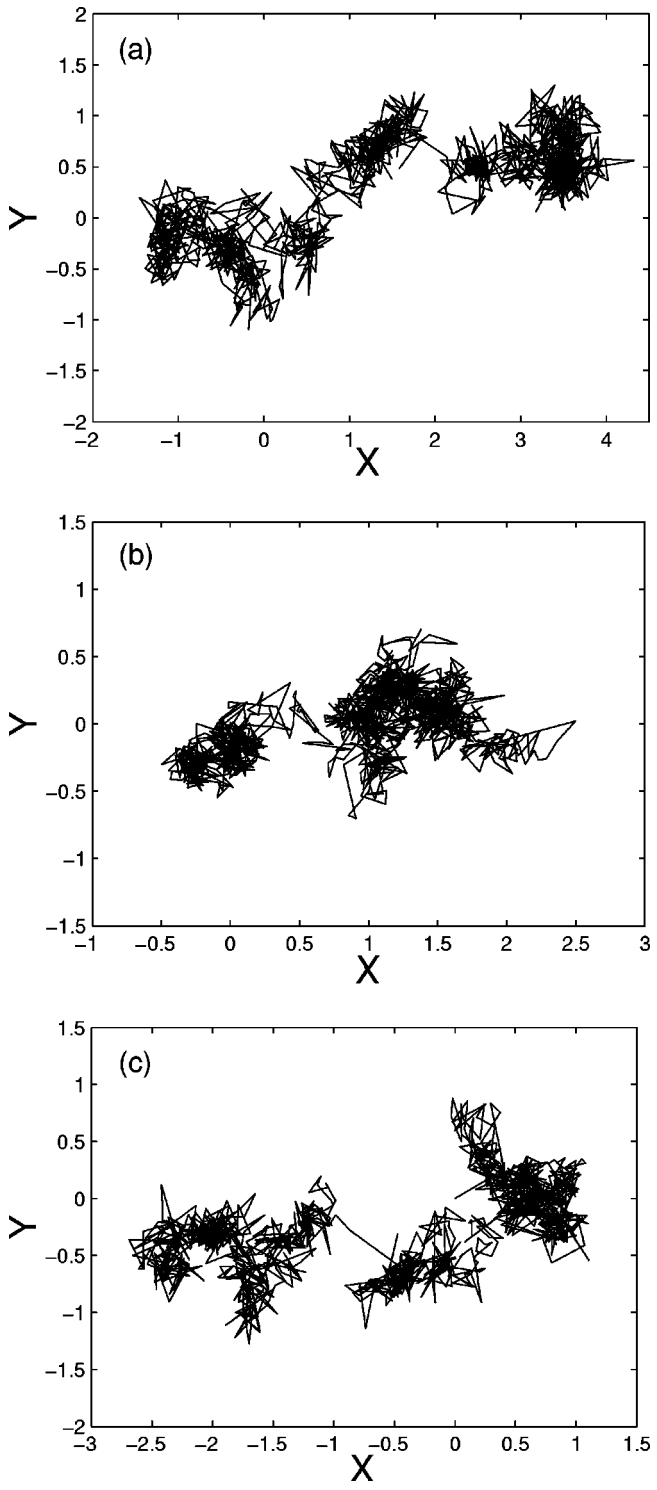

FIG. 5. (a) Projections into x-y plane of the trajectory of a typical nearest neighbor AB pair over a time interval $t=500\tau$. (b) Trajectory of the A particle of the same AB pair as in (a), within the same time window. (c) Trajectory of the B particle of the same AB pair. The time unit $\tau=2.2$ ps for argon units.

In Fig. 12(a) we show the angular distribution $g_{2,ang}(r_o,\theta;t)$ for the AA pair. We calculate the angular distribution with respect to the initial separation vector $\mathbf{r}_o$ and irrespective of the value of the separation at time t. The

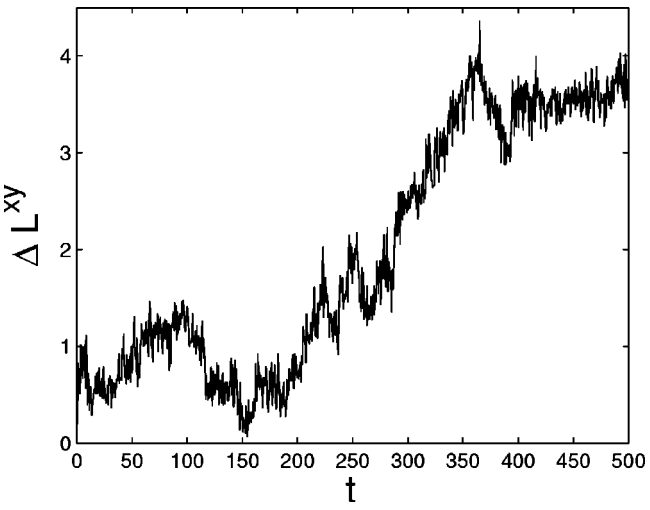

FIG. 6. The net displacement of an AB pair into x-y plane (ΔL^{xy}) as shown in Fig. 5(a), in the same time interval. Note that the displacement is quite large.

distribution which is a δ function at $t=0$ spreads more and more with time and eventually it reaches to a uniform distribution with zero slope. When we compare it to the distribution corresponding to the AB pair as shown in Fig. 12(b), we find that the approach to the uniform value is faster in case of the AB pair. This can be understood again in terms of the mobility of the B particles, which is more compared to the A particles. In Fig. 12(c) we show how the distribution for the BB pair changes with time. The relaxation is seen to be relatively slower at short times as compared to the AB pair.

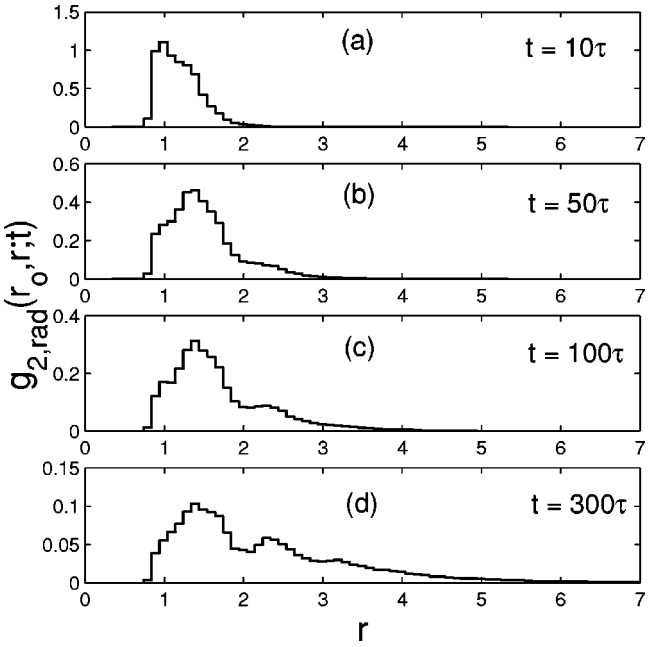

FIG. 7. The radial part of the time-dependent pair distribution function $g_{2,rad}(r_o,r;t)$ for the BB pair as a function of separation r at four different times: (a) $t=20\tau$, (b) $t=50\tau$, (c) $t=100\tau$, and (d) $t=300\tau$. The initial separation r_o corresponds to the first peak of $g_{BB}(r)$. Note that $g_{2,rad}(r_o,r;t)$ is scaled by $1/\sigma_{AA}^3$.

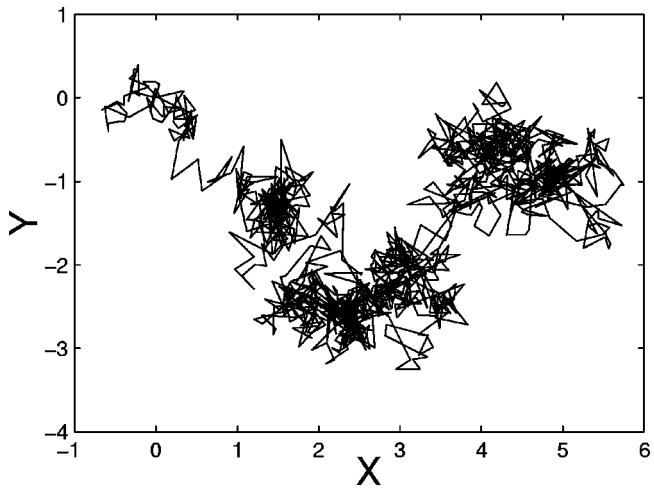

FIG. 8. Projections into x-y plane of the trajectory of a typical nearest neighbor BB pair over a time interval $t=500\tau$.

This can be understood in terms of the effective potential that is discussed later.

C. Relative diffusion: Mean-square relative displacement (MSRD)

In this section, we investigate the time dependence of the mean-square relative displacement $\langle|\mathbf{r}_{ij}(t)-\mathbf{r}_{ij}(0)|^2\rangle_{r_o}$, the simplest physical quantity associated with the pair motion, where the index i and j denote A and/or B particles and the subscript r_o indicates that the ensemble averaging is restricted to the pairs whose initial separation corresponds to

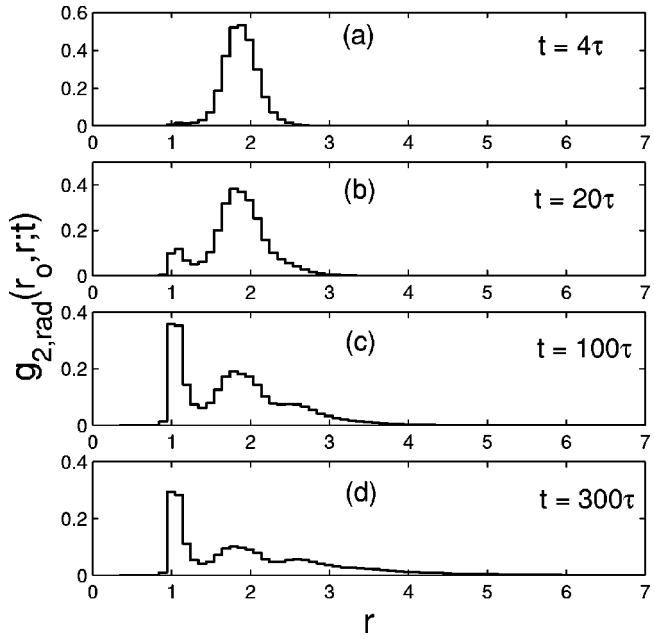

FIG. 9. The radial part of the pair distribution function $g_{2,rad}(r_o,r;t)$ for the AA pair at four different times: (a) $t=4\tau$, (b) $t=20\tau$, (c) $t=100\tau$, and (d) $t=300\tau$. Here the initial separation r_o is chosen at the second peak of $g_{AA}(r)$. The distribution function $g_{2,rad}(r_o,r;t)$ is scaled by $1/\sigma_{AA}^3$.

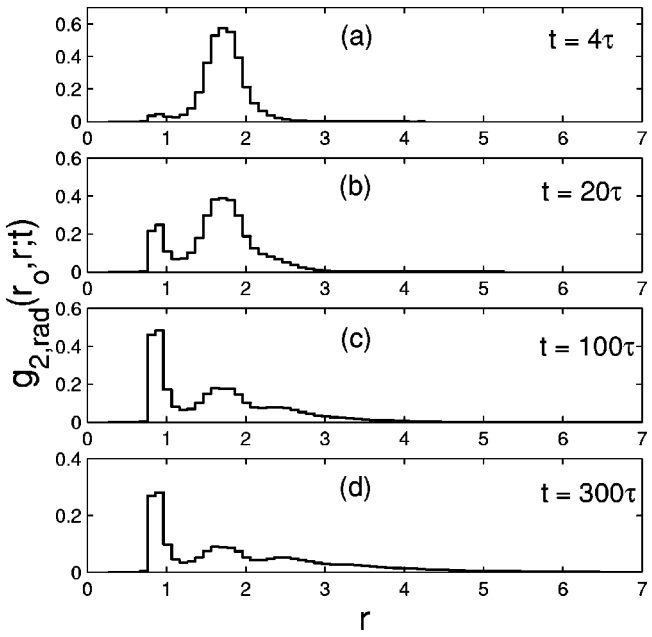

FIG. 10. The radial part of the pair distribution function $g_{2,rad}(r_o, r; t)$ for the AB pair at four different times: (a) $t = 4\tau$, (b) $t = 20\tau$, (c) $t = 100\tau$, and (d) $t = 300\tau$. Here the initial separation r_o corresponds to the second peak of $g_{AB}(r)$. The distribution function $g_{2,rad}(r_o, r; t)$ is scaled by $1/\sigma_{AA}^3$.

r_o [9]. First, we consider the case where the initial separations for the three pairs correspond to the first peak of the respective partial radial distribution functions (see Fig. 1). In other words, we consider first those pairs that were initially nearest neighbor pairs.

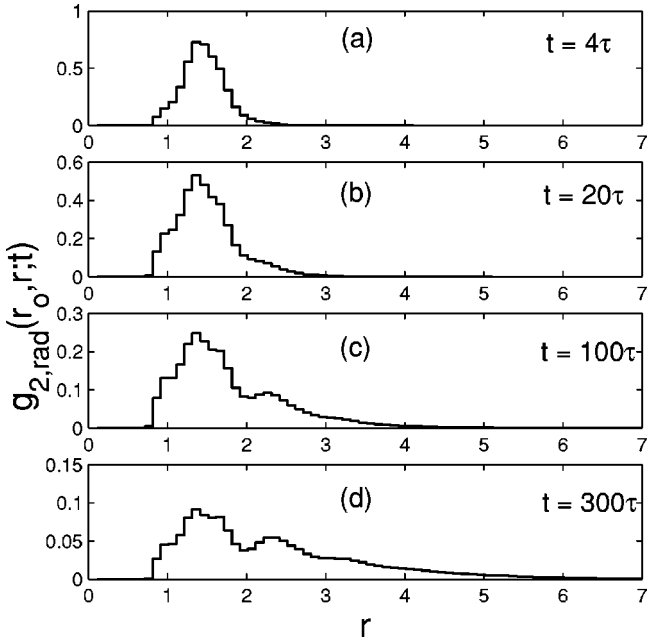

FIG. 11. The radial part of the pair distribution function $g_{2,rad}(r_o, r; t)$ for the BB pair at four different times: (a) $t = 4\tau$, (b) $t = 20\tau$, (c) $t = 100\tau$, and (d) $t = 300\tau$. Here, the initial separation r_o is chosen at the second peak of $g_{BB}(r)$. The distribution function $g_{2,rad}(r_o, r; t)$ is scaled by $1/\sigma_{AA}^3$.

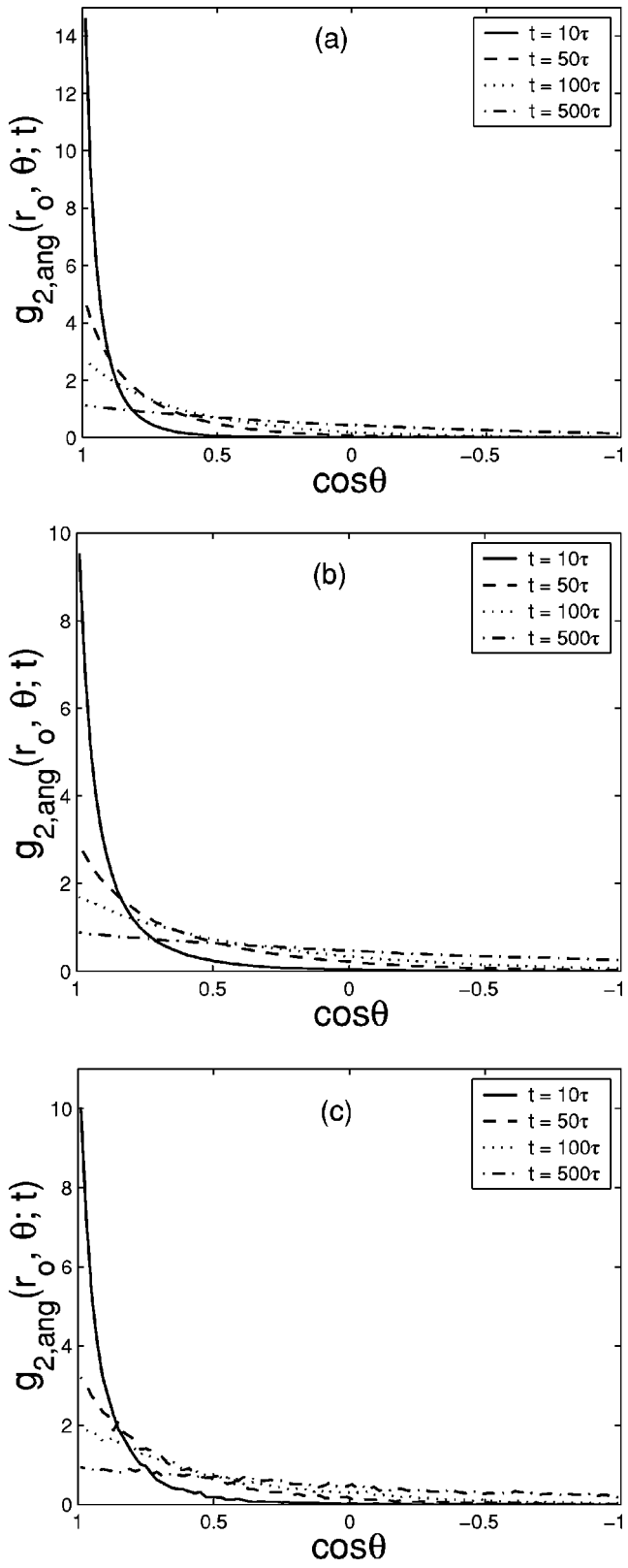

FIG. 12. (a) The angular part of the time-dependent pair distribution function $g_{2,ang}(r_o, \theta; t)$ for the AA pair at four different times. (b) $g_{2,ang}(r_o, \theta; t)$ for the AB pair. (c) $g_{2,ang}(r_o, \theta; t)$ for the BB pair. In all the three cases, we consider only those pairs which were initially separated at the nearest neighbor distance. For further details, see the text.

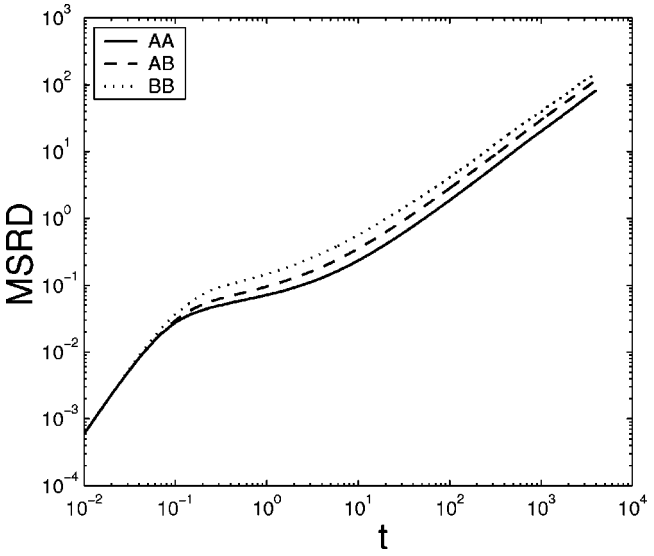

FIG. 13. Time dependence of the MSRD for the AA, AB, and BB pairs. The initial separation r_o of the three pairs corresponds to the first peak of the respective partial radial distribution functions. The solid line represents the result for the AA pair, the dashed line AB pair, and the dotted line for the BB pair. Note that MSRD is scaled by σ_{AA}^2. For the detailed discussion, see the text.

Figure 13 shows the result for the time dependence of the mean-square relative displacement (MSRD) of the three pairs. At long times the MSRD varies linearly with time. However, the evolution of MSRD with time differs for different pairs. As expected, the smaller size of the B particles and the weak BB interaction lead to a faster approach of the diffusive limit of BB pair separation. The time scale needed to reach the diffusive limit is shorter for the AB pair than that for the AA pair.

From the slope of the curves in the linear region, one can obtain the values of the relative diffusion constants D_R of the different pairs. The values thus obtained are the following (in reduced units): $D_R^{AA} \simeq 0.0032$, $D_R^{AB} \simeq 0.0048$, and $D_R^{BB} \simeq 0.0064$. One should note that even though the difference in size of the A and B particles is small, D_R^{BB} is almost twice of D_R^{AA}. At sufficiently long time, one would certainly expect the diffusion constant for the relative motion of a pair should be the sum of the individual diffusion constants of the two atoms obtained from the slope of the corresponding mean-square displacements at long time. Indeed, we find there is a good agreement.

An investigation of the behavior of MSRD is also performed for atomic pairs which were initially next nearest neighbors. When compared to the nearest neighbor pairs (Fig. 13), we find that the slope of the corresponding straight lines are almost identical, although in the case of AA and AB pairs, the diffusive limits are reached at shorter times. This has been shown in Fig. 14. One should remember that the AA and AB correlations are highest at the first coordination shell, whereas the highest BB correlations occur at the second coordination shell (see Fig. 1). Thus, at short time the increase in slope for the AA and AB pairs can be explained

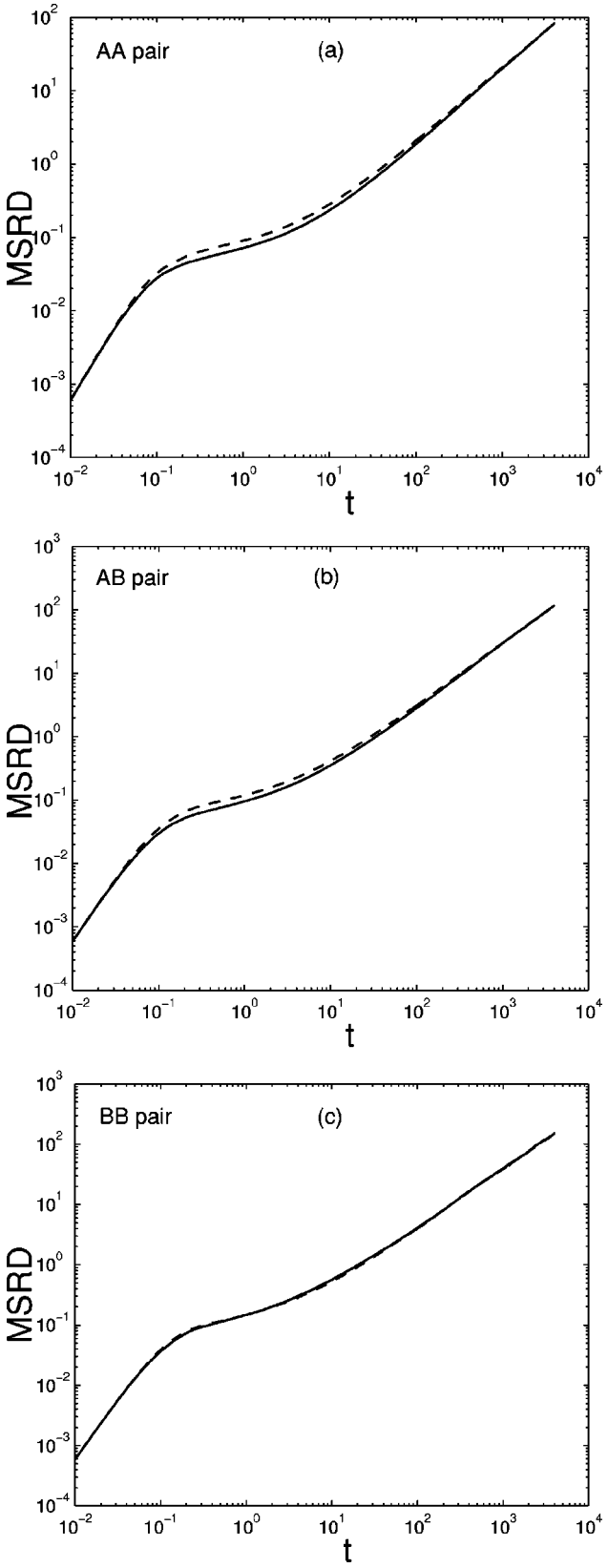

FIG. 14. (a) Comparison of the MSRD for the AA pair with different initial separations. The solid line represents the nearest neighbor AA pair and the dashed line represents the next nearest neighbor AA pair. (b) Same as in (a), but for the AB pair. (c) For the BB pair. In all the three cases MSRD is scaled by σ_{AA}^2.

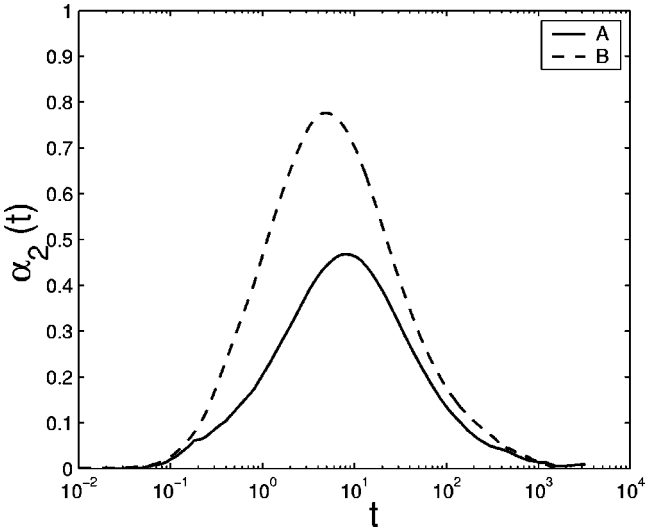

FIG. 15. The behavior of the non-Gaussian parameter $\alpha_2(t)$ as a function of time for the *A* and *B* particles. The solid line is for the *A* particles and the dashed line for the B particles. The unit of time is $\tau=\sqrt{m\sigma_{AA}^2/\epsilon_{AA}}=2.2$ ps if argon units are assumed.

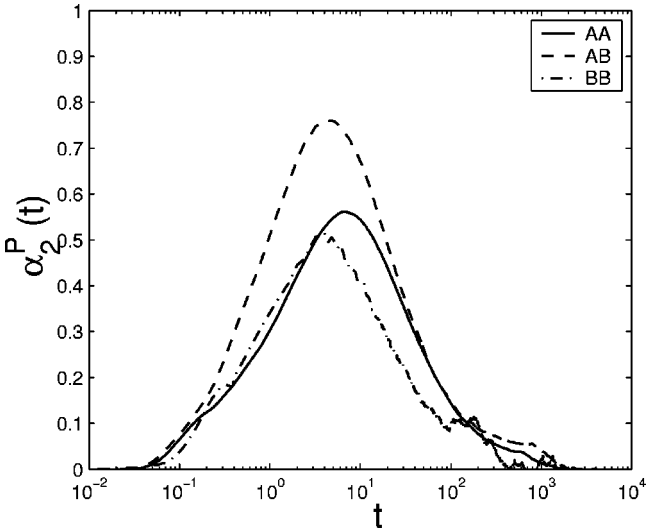

FIG. 16. The behavior of the non-Gaussian parameter $\alpha_2^P(t)$ as a function of time for the *AA*, *AB*, and *BB* pairs, initially separated at the nearest neighbor distance. The solid line represents the result for the *AA* pair, the dashed line for the *AB* pair, and the dot-dashed line for the *BB* pair. Here, time is scaled by $\tau=2.2$ ps for argon units.

in terms of the decrease in correlations at the second coordination shell.

D. The non-Gaussian parameter for the relative motion

In a highly supercooled liquid, the single-particle displacement distribution function $G_s(r,t)$ (known as the self-part of the van Hove correlation function) has an extended tail and is, in general, non-Gaussian. The deviation from the Gaussian behavior is often thought to reflect the presence of the transient inhomogeneities and can be characterized by the non-Gaussian parameter $\alpha_2(t)$ [22]

$$\alpha_2(t)=\frac{3\langle\Delta r^4(t)\rangle}{5\langle\Delta r^2(t)\rangle^2}-1, \tag{2}$$

where $\langle\Delta r^2(t)\rangle$ and $\langle\Delta r^4(t)\rangle$ are the second and fourth moments of $G_s(r,t)$, respectively. At intermediate time scale, $\alpha_2(t)$ increases with time and the maximum of $\alpha_2(t)$ occurs around the end of the β relaxation region. Only on the time scale of diffusion or the α relaxation, $\alpha_2(t)$ starts to decrease and finally at a very long time limit, it reaches to zero. $\alpha_2(t)$ calculated for the *A* and *B* particles are shown in Fig. 15. The maximum in $\alpha_2(t)$ is seen to shift slightly towards left and also the height of the maximum is higher for the *B* particles. This is a clear evidence that the *B* particles probe a much more heterogeneous environment than the *A* particles. This difference can be explained in terms of the smaller concentration of *B* particles, different sizes of the *A* and *B* particles and also from the fact that the interaction between the *B* particles is much weaker than that between the *A* particles [21,22].

Motivated by these findings for the single-particle displacement distribution function, we introduce a new non-Gaussian parameter for the pair dynamics, denoted by $\alpha_2^P(t)$. $\alpha_2^P(t)$ can be a measure of the deviation from the Gaussian behavior of the pair distribution function $g_2(\mathbf{r}_o,\mathbf{r};t)$. It can be defined as

$$\alpha_2^{P_{ij}}(t)=\frac{3\langle|\mathbf{r}_{ij}(t)-\mathbf{r}_{ij}(0)|^4\rangle_{r_o}}{5\langle|\mathbf{r}_{ij}(t)-\mathbf{r}_{ij}(0)|^2\rangle_{r_o}^2}-1 \quad (i,j=A \text{ and/or } B), \tag{3}$$

where $\langle|\mathbf{r}_{ij}(t)-\mathbf{r}_{ij}(0)|^2\rangle_{r_o}$ and $\langle|\mathbf{r}_{ij}(t)-\mathbf{r}_{ij}(0)|^4\rangle_{r_o}$ are the mean square relative displacement and mean quartic relative displacement of the ij pair. One should note that $\alpha_2^P(t)$ is identical to zero for a Gaussian pair distribution function.

In Fig. 16 we show the behavior of the $\alpha_2^{P_{ij}}$ as a function of time for the three different pairs. We again consider only those pairs that were initially nearest neighbors. The behavior observed for the three pairs is markedly different. The dynamics explored by the *BB* pair is seen to be less heterogeneous than the *AA* and *AB* pairs. Due to the smaller size of the *B* particles and the insignificant correlations among them, the *B* particles reach the average distribution faster, although it explores larger heterogeneity. The *AA* pair reaches the diffusive limit at a longer time scale than that for the *AB* pair, the *AB* pair explores more heterogeneous dynamics as is clearly evident from the difference in the maximum value of $\alpha_2^P(t)$.

IV. THEORETICAL ANALYSIS

For the motion of an atomic pair in a pure fluid, Haan [6] introduced a simple mean-field level equation of motion for the time-dependent pair distribution function g_2. This equation was shown to give a quantitatively correct description both at short and long times [15]. This treatment is mean field in the sense that the two atoms were assumed to diffuse

in an effective-force field of the surrounding particles given by the gradient of the potential of the mean force. The equation for g_2 was represented by a Smoluchowski equation and the correct short time description of g_2 was obtained only by introducing a *nonlinear time that is related to the mean-squared distance* (MSD) moved by a *single atom*. In other words, an *ad hoc* introduction of a time-dependent diffusion constant $D(t)$ in the equation of motion gives the correct description at short times.

In the view of its success for one-component liquid, we have performed similar mean-field model calculations for the binary mixture considered here. The generalization to binary mixture gives the following Smoluchowski equation for the different pairs:

$$\frac{\partial g_2^{ij}(\mathbf{r}_o,\mathbf{r};t)}{\partial \tau_{ij}} = \boldsymbol{\nabla}\cdot[\boldsymbol{\nabla} g_2^{ij}(\mathbf{r}_o,\mathbf{r};t) + \beta g_2^{ij}(\mathbf{r}_o,\mathbf{r};t)\boldsymbol{\nabla} W_{ij}(r)], \tag{4}$$

where indices i and j denote A and/or B particles. β is the inverse of Boltzmann's constant k_B times the absolute temperature T. $W_{ij}(r)$ is the potential of mean force (effective potential) between i and j particles given by

$$W_{ij}(r) = -k_B T \ln g_{ij}(r), \tag{5}$$

where $g_{ij}(r)$ is the partial radial distribution function. In Eq. (4), the "time" τ_{ij} is defined by

$$\tau_{ij} = \frac{1}{6}\langle|\mathbf{r}_{ij}(t)-\mathbf{r}_{ij}(0)|^2\rangle_{r_o}$$

$$\approx \frac{1}{6}[\langle|\mathbf{r}_i(t)-\mathbf{r}_i(0)|^2\rangle + \langle|\mathbf{r}_j(t)-\mathbf{r}_j(0)|^2\rangle], \tag{6}$$

where $\langle|\mathbf{r}_{ij}(t)-\mathbf{r}_{ij}(0)|^2\rangle_{r_o}$ is the MSRD of "ij" pair. Note that an approximation is made in the above equation by neglecting the cross correlation between the two particles (i and j) and the MSRD is replaced by the sum of individual particle's MSD.

Now the integration of the $g_2^{ij}(\mathbf{r}_o,\mathbf{r};t)$ over the solid angles $\hat{\Omega}_o$ and $\hat{\Omega}$ corresponding to the initial and final positions, respectively, gives the radial part of the full distribution function [the zeroth-angular moment of $g_2^{ij}(\mathbf{r}_o,\mathbf{r};t)$]

$$g_{2,rad}^{ij}(r_o,r;t) = \frac{1}{4\pi}\int d\hat{\Omega}_o d\hat{\Omega} g_2^{ij}(\mathbf{r}_o,\mathbf{r};t). \tag{7}$$

Note that the normalization of this function is

$$\int_0^\infty dr r^2 g_{2,rad}^{ij}(r_o,r;t) = 1. \tag{8}$$

The equation of motion for $g_{2,rad}^{ij}(r_o,r;t)$ [derived from Eq. (4)] is solved numerically (by Crank-Nicolson method) for the different pairs and the results obtained from this model calculations are compared with the simulation results. The partial radial distribution functions $g_{ij}(r)$ and the mean-square displacement of the A and B particles (required as input) are obtained from the present simulation.

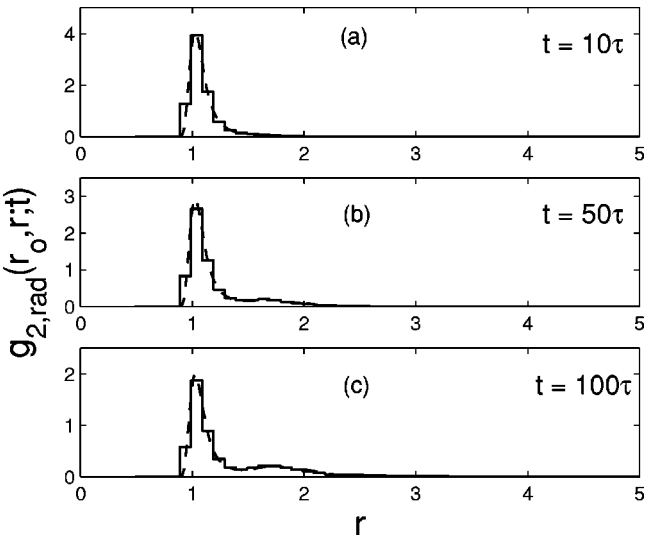

FIG. 17. The simulated distribution $g_{2,rad}(r_o,r;t)$ for the AA pair is compared with the mean-field model calculations at three different times: (a) $t=10\tau$, (b) $t=50\tau$, and (c) $t=100\tau$. The initial separation r_o corresponds to the first maximum of $g_{AA}(r)$. The histogram represents the simulation results and the dashed line represents the results of the model calculations. Note that $g_{2,rad}(r_o,r;t)$ is scaled by $1/\sigma_{AA}^3$ and the time unit $\tau=2.2$ ps if argon units are assumed.

Figures 17 and 18 compare model calculations with the simulated distribution functions for the AA and AB nearest neighbor pair. The time evolution of the distributions is described well by the simple mean-field model. The under-

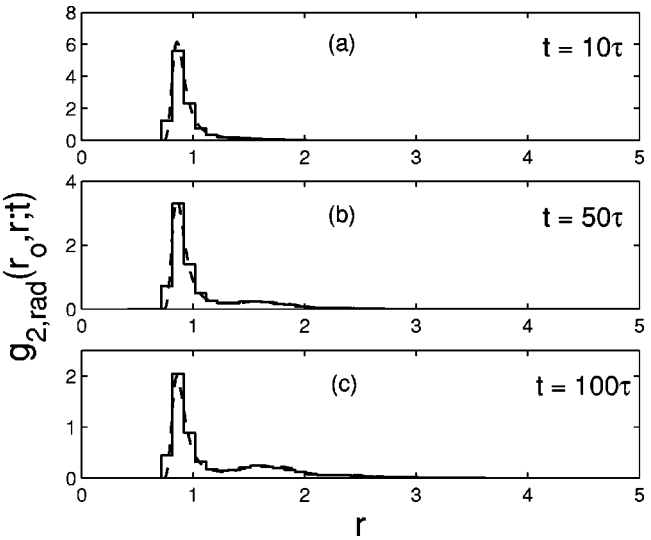

FIG. 18. The simulated distribution $g_{2,rad}(r_o,r;t)$ for the AB pair is compared with the mean-field model calculations at three different times: (a) $t=10\tau$, (b) $t=50\tau$, and (c) $t=100\tau$. The initial separation r_o corresponds to the first maximum of $g_{AB}(r)$. The histogram represents the simulation results and the dashed line represents the results of the model calculations. The distribution function $g_{2,rad}(r_o,r;t)$ is scaled by $1/\sigma_{AA}^3$.

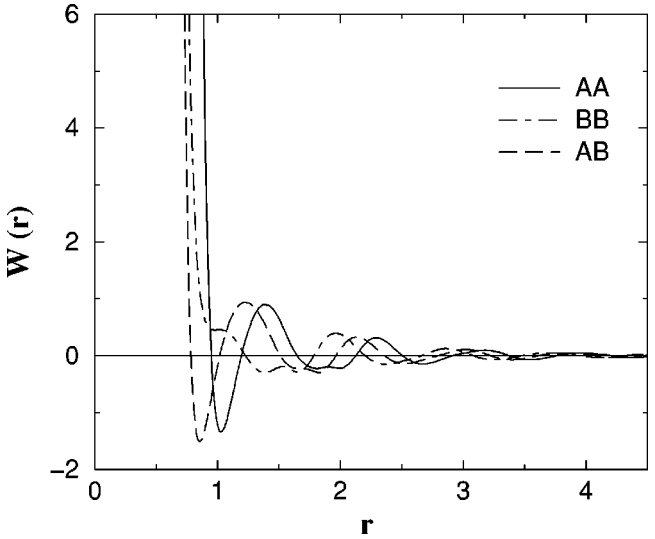

FIG. 19. The potential of mean force $W(r)$ for the AA, AB, and BB pairs in the Kob-Andersen model at the reduced pressure $P^*=20$ and the reduced temperature $T^*=1.0$. The solid line represents for the AA pair, the dashed line for the AB pair, and the dot-dashed line for the BB pair. Note that $W(r)$ is scaled by ϵ_{AA}.

lying effective-potential energy surfaces are plotted in Fig. 19. Thus, relative diffusion in these cases can be considered as overdamped motion in an effective potential, which takes place mainly via hopping (as shown in Figs. 3 and 5) that governs the time evolution of the distributions for the AA and AB pairs.

Unfortunately, the good agreement observed above between simulation and theory for the AA and AB pairs does not extend to the BB pair. This is shown in Fig. 20. As the

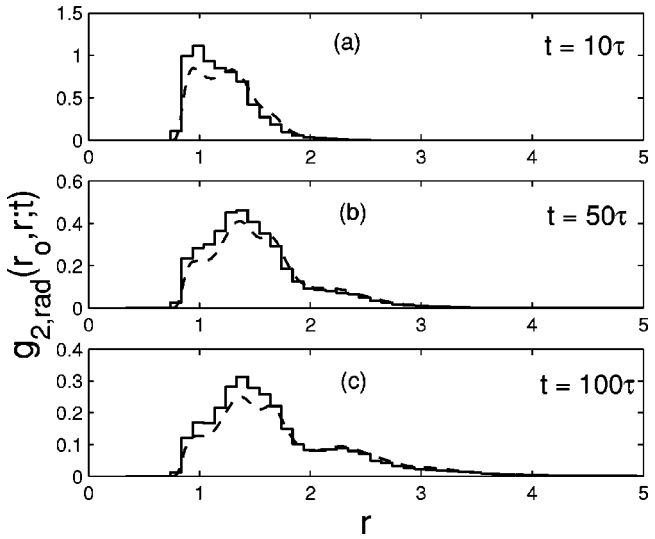

FIG. 20. The simulated distribution $g_{2,rad}(r_o,r;t)$ for the BB pair is compared with the mean-field model calculations at three different times: (a) $t=10\tau$, (b) $t=50\tau$, and (c) $t=100\tau$. The initial separation r_o corresponds to the first peak of $g_{BB}(r)$. The histogram represents the simulation results and the dashed line represents the results of the model calculations. The distribution function $g_{2,rad}(r_o,r;t)$ is scaled by $1/\sigma_{AA}^3$.

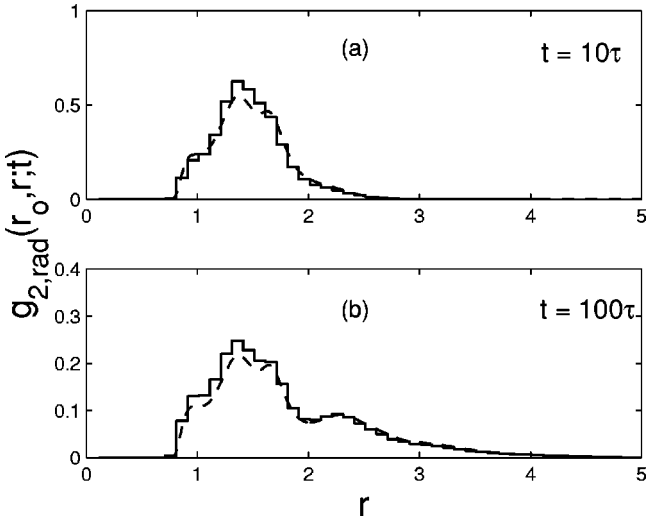

FIG. 21. The simulated distribution $g_{2,rad}(r_o,r;t)$ for the BB pair is compared with the mean-field model calculations at two different times: (a) $t=10\tau$ and (b) $t=100\tau$. Here the initial separation r_o corresponds to the second peak of $g_{BB}(r)$. The histogram again represents the simulation results and the dashed line represents the results of the model calculations. Note that $g_{2,rad}(r_o,r;t)$ is scaled by $1/\sigma_{AA}^3$. For further details, see the text.

number of B particles present in the system is much less (20%) and the interparticle interaction is weak, the effective potential for a B atom interacting with a nearest neighbor atom is unfavorable (see Fig. 19). Consequently, the nearest neighbor BB pair executes highly anharmonic motion. Thus, the fluctuations about the mean-force field experienced by the BB pair are large and important. These fluctuations are neglected here, as in other mean-field level description.

The extension of the calculations to the case of next nearest neighbor pairs has also been carried out and compared with the simulated distributions. It should be noted that as compared to the nearest neighbor pairs, the AA and AB pairs now execute motions in a relatively weak, shallow potential, whereas the motions of the BB pair takes place in a relatively strong, bound potential well (see Fig. 19). Thus, for the BB pair, one expects a better agreement with the simulated distributions as compared to the earlier case (nearest neighbor BB pairs). Indeed, the agreement is better for the BB pair as shown in Fig. 21 (compare with Fig. 20). We have found that the MF model provides a good description of the dynamics of the AA and AB pairs, although the agreement is not as satisfactory as for the nearest neighbor pairs.

Thus, it is evident that the MF description for the time-dependent pair distribution functions is reasonably good for the AA and AB pairs. Simulation results have shown that the relative diffusion of an AB pair is higher than that for an AA pair. We noted that this is due to the more frequent hopping of the B particles than the A particles. Our main objective now is to see whether the frequent jump motions of the B particles, as predicted by the simulations, can be explained in terms of the MF model described above.

We have performed an approximate calculation to get an estimate of the transition rate between the first two adjacent minima in the effective potential energy surface of the AA

and AB pairs (see Fig. 19). In other words, the rate of crossing from the deep minima located at the nearest neighbor pairs to the adjacent minima (corresponds to the next nearest neighbors) is calculated. As the motion of a pair in the effective potential is treated by a Smoluchowski equation, we use the corresponding rate expression in the overdamped limit to calculate the escape rate. Thus, we have an expression for the escape rate given by [36]

$$k_S \cong \frac{\omega_{min}\omega_{max}}{2\pi\zeta}\exp\left(-\frac{\Delta W}{k_B T}\right), \tag{9}$$

where $\Delta W = W(r_{max}) - W(r_{min})$ is the Arrhenius activation energy and ω_{min}, ω_{max} are the frequency at the minima r_{min} and maxima r_{max} in the effective potential $W(r)$, respectively. The diffusion coefficient D is related to the friction ζ by $D = k_B T/\zeta$.

Thus, to calculate the transition rate we need to know the values of the frequency ω_{min}, ω_{max}, and the barrier height ΔW, which are different for the AA and AB pairs. For the AA pair, these parameters are found to be $\omega^*_{min}(=\omega_{min}\tau) \simeq 16.5$, $\omega^*_{max} \simeq 6.5$, and $\Delta W_{AA} \simeq 2.25 k_B T$, whereas for the AB pair they are $\omega^*_{min} \simeq 17.8$, $\omega^*_{max} \simeq 7.4$, and $\Delta W_{AB} \simeq 2.45 k_B T$. The relative diffusion of the two pairs is (in reduced units) $D_R^{AA} \simeq 0.0032$ and $D_R^{AB} \simeq 0.0048$. Using all these parameters, the escape rate calculated for the AA and AB pairs is (in reduced units) $k_S^{AA} \simeq 5.9 \times 10^{-3}$ and $k_S^{AB} \simeq 8.8 \times 10^{-3}$, respectively (in terms of time τ, which is equal to 2.2 ps for argon units).

Even though the barrier height $\Delta W_{AB} > \Delta W_{AA}$, the transition rate for the AB pair is larger than that for the AA pair. Thus, the jump motions are much more frequent for the AB pair due to the large diffusion of the B particles in the potential energy surface (which mainly occurs via hopping).

V. CONCLUSIONS

Let us first summarize the main results of this study. We have presented the molecular dynamics simulation results for the time-dependent pair distribution functions in a strongly nonideal glass-forming binary Lennard-Jones mixture. In addition, a mean-field description of the pair dynamics is considered and the comparison is made with the simulated distributions. The main goal of this investigation was to explore the dynamics of the supercooled liquids in a more collective way by following the *relative* motion of the atoms rather than *absolute* motion of the atoms. We find that the three pairs (AA, BB, and AB) behave differently. The analysis of the trajectory shows a clear evidence of the jump motions for all the three pairs.

The relative diffusion constant of the BB pair (D_R^{BB}) is almost twice the value for the AA pair (D_R^{AA}). This clearly suggests the importance of the jump dynamics for the B particles and indeed, we find that the motion of the B particles is mostly discontinuous in nature, while the A particles show occasional hopping. The dynamic inhomogeneity present in a supercooled liquid is generally characterized by the well-known non-Gaussian parameter $\alpha_2(t)$, which describe the deviations from the Gaussian behavior in the motion of a single atom. In this paper, we have generalized this concept and introduced a non-Gaussian parameter for the pair dynamics [$\alpha_2^P(t)$] to measure the deviations from the Gaussian behavior in the relative motion of the atoms. At intermediate times, all the three pair distribution functions for the three pairs show significant deviations from the Gaussian behavior with different degrees.

It is found that for the nearest neighbor AA and AB pairs, which are confined to a strong effective potential and merely makes anharmonic motions in it, the dynamics can be treated at the mean-field level. However, as the motion of a nearest neighbor BB pair is highly anharmonic, one must include the effects of the fluctuations about the mean-force field in order to get a correct description of the dynamics.

While the mean-field treatment provides reasonably accurate description of pair dynamics (at least for AA and AB pairs), it must be supplemented with the time-dependent diffusion coefficient $D(t)$. This is a limitation of the mean-field approach because at present we do not have any theoretical means to calculate $D(t)$ from first principles. The mode coupling theory does not work because it neglects hopping which is the dominant mode of mass transport in deeply supercooled liquids, even when the system is quite far from the glass transition. As we discussed recently, hopping can be coupled to anisotropy in the local stress tensor [26]. The calculation of the latter is also nontrivial. Work in this direction is under progress.

ACKNOWLEDGMENTS

This work was supported in part by the Council of Scientific and Industrial Research (CSIR), India and the Department of Science and Technology (DST), India. One of the authors (R.K.M) thanks the University Grants Commission (UGC) for providing financial support.

[1] I. Oppenheim and M. Bloom, Can. J. Phys. **39**, 845 (1961).
[2] J.A. Bucaro and T.A. Litovitz, J. Chem. Phys. **54**, 3846 (1971); A.J.C. Ladd, T.A. Litovitz, and C.J. Montrose, *ibid.* **71**, 4242 (1979); A.J.C. Ladd, T.A. Litovitz, J.H.R. Clarke, and L.V. Woodcock, *ibid.* **72**, 1759 (1980).
[3] M.S. Miller, D.A. McQuarrie, G. Birnbaum, and J.D. Poll, J. Chem. Phys. **57**, 618 (1972).
[4] S.A. Adelman, Adv. Chem. Phys. **53**, 61 (1983).
[5] J.T. Hynes, R. Kapral, and G.M. Torrie, J. Chem. Phys. **72**, 177 (1980).
[6] S.W. Haan, Phys. Rev. A **20**, 2516 (1979).
[7] C.D. Boley and G. Tenti, Phys. Rev. A **21**, 1652 (1980).
[8] U. Balucani and R. Vallauri, Physica A **102**, 70 (1980); Phys. Lett. A **76**, 223 (1980); Chem. Phys. Lett. **74**, 75 (1980).
[9] U. Balucani, R. Vallauri, C.S. Murthy, T. Gaskell, and M.S. Woolfson, J. Phys. C **16**, 5605 (1983); U. Balucani, R. Val-

lauri, T. Gaskell, and M. Gori, *ibid.* **18**, 3133 (1985).
[10] H. Posch, F. Vesely, and W. Steele, Mol. Phys. **44**, 241 (1981).
[11] G.T. Evans and D. Kivelson, J. Chem. Phys. **85**, 7301 (1986).
[12] Ten-Ming Wu and S.L. Chang, Phys. Rev. E **59**, 2993 (1999).
[13] G. Srinivas, A. Mukherjee, and B. Bagchi, J. Chem. Phys. **114**, 6220 (2001).
[14] R.K. Murarka and B. Bagchi, J. Chem. Phys. **117**, 1155 (2002).
[15] J.G. Saven and J.L. Skinner, J. Chem. Phys. **99**, 4391 (1993); M.D. Stephens, J.G. Saven, and J.L. Skinner, *ibid.* **106**, 2129 (1997).
[16] A.D. Santis, A. Ercoli, and D. Rocca, Phys. Rev. E **57**, R4871 (1998); Phys. Rev. Lett. **82**, 3452 (1999).
[17] M.D. Ediger, C.A. Angell, and S.R. Nagel, J. Phys. Chem. **100**, 13 200 (1996); C.A. Angell, Science **267**, 1924 (1995); C.A. Angell, K.L. Ngai, G.B. McKenna, P.F. McMillan, and S.W. Martin, J. Appl. Phys. **88**, 3113 (2000); P.G. Debenedetti and F.H. Stillinger, Nature (London) **410**, 259 (2001).
[18] A. Mukherjee, S. Bhattacharyya, and B. Bagchi, J. Chem. Phys. **116**, 4577 (2002).
[19] M.D. Ediger, Annu. Rev. Phys. Chem. **51**, 99 (2000).
[20] E.R. Weeks, J.C. Crocker, A.C. Levitt, A. Schofield, and D.A. Weitz, Science **287**, 627 (2000); W.K. Kegel and A. van Blaaderen, *ibid.* **287**, 290 (2000); L.A. Deschenes and D.A. Vanden Bout, *ibid.* **292**, 255 (2001).
[21] W. Kob and H.C. Andersen, Phys. Rev. E **51**, 4626 (1995); W. Kob and H.C. Andersen, Phys. Rev. Lett. **73**, 1376 (1994).
[22] W. Kob, C. Donati, S.J. Plimpton, P.H. Poole, and S.C. Glotzer, Phys. Rev. Lett. **79**, 2827 (1997); C. Donati, S.C. Glotzer, P.H. Poole, W. Kob, and S.J. Plimpton, Phys. Rev. E **60**, 3107 (1999); K. Vollmayr-Lee, W. Kob, K. Binder, and A. Zippelius, J. Chem. Phys. **116**, 5158 (2002).
[23] S. Sastry, P.G. Debenedetti, and F.H. Stillinger, Nature (London) **393**, 554 (1998).
[24] B. Doliwa and A. Heuer, Phys. Rev. Lett. **80**, 4915 (1998); J. Qian, R. Hentschke, and A. Heuer, J. Chem. Phys. **110**, 4514 (1999).
[25] C. Donati, J.F. Douglas, W. Kob, S.J. Plimpton, P.H. Poole, and S.C. Glotzer, Phys. Rev. Lett. **80**, 2338 (1998).
[26] S. Bhattacharyya and B. Bagchi, Phys. Rev. Lett. **89**, 025504 (2002).
[27] S. Bhattacharyya, A. Mukherjee, and B. Bagchi, J. Chem. Phys. **117**, 2741 (2002).
[28] C. Oligschleger and H.R. Schober, Phys. Rev. B **59**, 811 (1999).
[29] H. Miyagawa, Y. Hiwatari, B. Bernu, and J.P. Hansen, J. Chem. Phys. **88**, 3879 (1988).
[30] D. Caprion, J. Matsui, and H.R. Schober, Phys. Rev. Lett. **85**, 4293 (2000).
[31] M. P. Allen and D. J. Tildesley, *Computer Simulation of Liquids* (Oxford University Press, Oxford, 1987).
[32] G.J. Martyna, D.J. Tobias, and M.L. Klein, J. Chem. Phys. **101**, 4177 (1994); H.C. Andersen, *ibid.* **72**, 2384 (1980); S. Nose, Mol. Phys. **52**, 255 (1984); W.G. Hoover, Phys. Rev. A **31**, 1695 (1985).
[33] G.J. Martyna, M.E. Tuckerman, and M.L. Klein, J. Chem. Phys. **97**, 2635 (1992).
[34] M.E. Tuckerman, G.J. Martyna, and B.J. Berne, J. Chem. Phys. **97**, 1990 (1992).
[35] G.J. Martyna, M.E. Tuckerman, D.J. Tobias, and M.L. Klein, Mol. Phys. **87**, 1117 (1996).
[36] R. Zwanzig, *Non-equilibrium Statistical Mechanics* (Oxford University Press, New York, 2001).